University College London

Project Report

Understanding Cosmic Muons Through Simulation

PHAS0097 - MSci Physics Project

Hugo Neely

MSci Natural Sciences (Physics and Physical Chemistry)

First Supervisor: Dr. Andreas Korn

Second Supervisor: Prof. Ryan Nichol

Word count: 7468

25th March 2022

UCL DEPARTMENT OF PHYSICS & ASTROMOMY

Submission of coursework for Physics and Astronomy course PHAS0097/PHAS0048
2020/21

Please sign, date and return this form with your coursework by the specified deadline.

DECLARATION OF OWNERSHIP

I confirm that I have read and understood the guidelines on plagiarism, that I understand the meaning of plagiarism and that I may be penalised for submitting work that has been plagiarised.

I confirm that all work will also be submitted electronically and that this can be checked using the JISC detection service, Turnitin®.

I declare that all material presented in the accompanying work is entirely my own work except where explicitly and individually indicated and that all sources used in its preparation and all quotations are clearly cited.

Should this statement prove to be untrue, I recognise the right of the Board of Examiners to recommend what action should be taken in line with UCL's regulations.

Signed 

PrintName HUGO NEELY

Dated 25/03/2022

Title	Date Received	Examiner	Examiner's Signature	Mark

Abstract

The measurement of the muon lifetime is a common experiment in undergraduate laboratories due to its accessibility and the range of concepts it may be used to introduce. This project has focused upon constructing an efficient and open Monte Carlo simulation of one such setup, aiding understanding of the results of this experiment and providing methods for data analysis and presentation. After a review of the underlying physics being simulated and the Monte Carlo techniques used, the methods used to simulate the detection of the cosmic muon flux are described along with an analysis of the efficiency and accuracy of the simulation. The simulation is shown to be capable of reproducing the expected average muon lifetime in matter to 2 significant figures, however further improvements upon the accuracy of this value are severely limited by systematic error produced by an erroneous energy loss algorithm.

Contents

1 Introduction

Cosmic rays are a group of particles composed mostly of atomic nuclei, approximately 90% hydrogen, 9% helium and 1% heavier nuclei [1] which propagate through space, often with very high energies. These particles constantly enter Earth's atmosphere, producing showers of energetic subatomic particles which propagate to sea level and below. Since their discovery in 1912 by Victor Hess [2], cosmic rays have been involved in a large number of scientific advances. Key discoveries using cosmic rays include the muon in 1936 [3], the positron in 1932 [4] which confirmed the existence of antimatter, and the discovery of neutrino oscillation in 1998 which demonstrated that neutrinos have mass [5]. One of their most useful common applications today is in physics education, where cosmic rays are used as an accessible and non-harmful source of high-energy particles. The development of low-cost accessible detectors such as [6] and [7] has allowed the measurement of cosmic rays to become a staple of undergraduate laboratory experiments and find use in physics outreach setups such as [8] and [9].

This project has aimed to produce a Monte Carlo simulation of one of the most common cosmic ray experiments - the measurement of the muon lifetime. Simulations of this sort are useful as they provide a better understanding of the results of the experiment by allowing inspection of important variables such as muon energy loss within the detector that are not easily measurable in an undergraduate laboratory setting. Additionally, these simulations can provide a method to simulate data when lab access is not possible and provide tools to quickly analyse and visualise data. The accuracy of the simulation has been inspected in detail by determining the maximum obtainable accuracy of its results and how these depend upon the simulation setup specified by the user. The efficiency of the simulation has also been inspected to ensure the simulation is capable of producing an acceptable number of events in a short span of time.

2 Background

2.1 Cosmic muons

Cosmic muon is a term used to refer to muons produced in the showers of subatomic particles created when cosmic rays interact with atoms in the upper atmosphere. A muon is a subatomic particle which is almost identical to an electron, but with 206.768 times more mass and with a differing lepton family number [10]. These two differences cause the muon to behave distinctly differently from the electron in many ways. The most relevant difference for this project is the muon's ability to decay via the weak force - the Feynman diagram for this process is shown below in Figure 1:

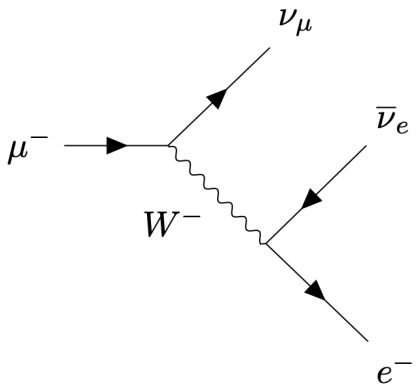

Figure 1: Feynman diagram for muon decay ($\mu \rightarrow e^- + \nu_\mu + \bar{\nu_e}$)

The resulting lifetimes of muons are exponentially distributed with an average value of $\tau_\mu = (2.1969803 \pm 0.0000022) \times 10^{-6}$s [11]. This quantity is important to HEP due to its links to the parameters of the weak force and has been measured to very high precision in experiments discussed in subsection 2.2. Interestingly, this parameter appears to reduce when muons decay in matter, though this reduction is not present for antimuons. As muons are negatively charged and have a different lepton family quantum number to electrons, they may form muonic atoms (atoms with muons in the place of electrons) with the nuclei of atoms in matter. When muons reach the ground state of the atom, they may interact with protons in the nucleus, producing neutrons and neutrinos ($\mu^- + p \rightarrow n + \nu_\mu$) in a process known as muon capture [12]. This results in a modification of the negative muon's decay rate: $\lambda_- = \lambda_+ + \lambda_c$, where $\lambda_+ = 1/\tau_\mu$ and λ_c is the rate

of muon capture. λ_c increases as a function of the charge of the nucleus of muonic atom, hence causing the muon capture rate to be different depending upon the material it is found in. The most relevant muon capture rate to this project is muon capture upon carbon, which has been measured to be $\lambda_c(^{12}\mathrm{C}) = 6.57^{+0.11}_{-0.21} \times 10^3 \mathrm{s}^{-1}$ [13] producing an effective muon lifetime in carbon of $1/\lambda_- = 2.17^{+0.04}_{-0.07} \times 10^{-6}\mathrm{s}$.

A further relevant property of the muon is its ability to penetrate large distances of matter losing very little energy. Particles lose energy via a variety of processes while passing through matter in a manner summarised by the Bethe-Bloch equation:

$$\left\langle -\frac{dE}{dx} \right\rangle = Kz^2 \frac{Z}{A} \frac{1}{\beta^2} \left[\frac{1}{2} \ln \frac{2m_e c^2 \beta^2 \gamma^2 W_{max}}{I^2} - \beta^2 - \frac{\delta(\beta\gamma)}{2} \right] \tag{1}$$

Where K is a combination of constants ($K \approx 0.307 \mathrm{MeVg}^{-1}\mathrm{cm}^2$), Z, A and I are the atomic number, mass number, and mean excitation potential of the material, $W_{max} = \frac{2m_e c^2 \beta^2 \gamma^2}{1+2\gamma m_e/M+(m_e/M)^2}$ is the maximum energy lost in a single collision, and z, β, γ and M are the charge, velocity relative to the speed of light, Lorentz factor, and mass of the particle in question. One of the main processes that causes high energy electrons to lose energy in matter is bremsstrahlung (or 'breaking radiation') - a process in which charged particles emit photons after being decelerated or deflected by the electric fields of nuclei and other charged particles. Electrons are highly likely to undergo this process, preventing them from travelling large distances in matter. For muons, bremsstrahlung is a factor of $(\frac{m_e}{m_\mu})^2 \approx 10^{-5}$ less likely to occur, causing the energy lost by muons via this process to be minimal [1]. Additionally, their mass causes muons to lose a smaller proportion of their momentum in collisions with electrons (ionisation energy loss). Overall these effects cause muons to lose very little energy while propagating through matter making them one of the most penetrating charged particles. This is demonstrated well by cosmic muons, which are typically produced at a height of 15km from sea level, have an appreciable (though very small) flux in underground laboratories such as SNOlab, which is situated at a depth of 2km below the surface [14].

The processes that produce cosmic muons lead to a number of unique properties of the cosmic muon flux. Cosmic muons are produced through a cascade of interactions beginning in the upper atmosphere, where primary cosmic rays interact with nuclei in atoms to produce hadrons. The most common of these hadrons are neutrons, protons, pions and kaons. Pions decay to produce mostly

photons if neutral ($\pi^0 \rightarrow \gamma\gamma$, $Br \approx 98.8\%$) or muons and neutrinos if charged ($\pi^{\pm} \rightarrow \mu^{\pm} + \nu_{\mu}/\bar{\nu_{\mu}}$, $Br \approx 99.9\%$) [15]. These decays are the main source of cosmic muons in the atmosphere, along with the decay of charged kaons ($K^{\pm} \rightarrow \mu^{\pm} + \nu_{\mu}/\bar{\nu_{\mu}}, Br \approx 63.6\%$). As the majority of primary cosmic rays are positively charged nuclei, there is a relative abundance of μ^+ rather than μ^-. This abundance is quantified by the cosmic muon charge ratio $\rho = N_+/N_-$, where N_+ and N_- are the observed numbers of μ^+ and μ^- respectively. This quantity has been measured to be $\rho = 1.2766 \pm 0.0032$ (statistical) ± 0.0032 (systematic) for muons with momentum less than 100GeV/c [16].

On average, the total muon flux at sea level is approximately 1μ cm^{-2} min^{-1} [15]. Energy loss of muons in the atmosphere causes this flux to be dependent upon both the muon energy and their zenith approach angle. The zenith angle (ϕ) is defined as the angle between the downward vertical direction and the muons path. The greatest intensity of muons is found when muons are travelling vertically downwards ($\phi = 0$) and reduces as ϕ increases, following a distribution which is well approximated by $I(\phi) = I(\phi = 0)\cos^2(\phi)$ [1]. The dependence upon the zenith angle stems from the increased distances muons must travel to reach sea level at larger values of ϕ. Muons travelling with a greater value of ϕ pass through a longer stretch of atmosphere to reach the Earth's surface and be detected. These muons will therefore lose more energy and take longer to reach the detector, increasing the proportion of muons that are stopped or decay before reaching sea level. As the reduction in flux at high zenith angles is largely due to energy loss, there is a correlation between zenith angle and muon energy: while larger ϕ produces a reduced flux, this flux contains a greater proportion of high energy muons. The flux as a function of muon momentum can be described to a good level of detail by the following equation [17]:

$$I(p) = I(\phi)N(E_0 + p)^{-n}(1 + \frac{p}{\epsilon})^{-1} \tag{2}$$

Where $N = (n-1)(E_0 + E_c)^{n-1}$ is a normalisation constant, E_0 is a parameter accounting for energy loss due to interactions with air, ϵ is a parameter accounting for the finite lifetime of parent hadrons and n is the power of the distribution.

2.2 Studies of the muon lifetime

The muon lifetime is an extremely important parameter for HEP due to its relation with the Fermi coupling constant G_F, shown below in Equation 3. This constant determines the strength of the weak interaction, and is one of the empirical parameters of the standard model which must be determined for the theory to make predictions.

$$\frac{1}{\tau_\mu} = \frac{G_F^2 m_\mu^2}{192\pi^3}(1 + \Delta q) \tag{3}$$

Due to this, there is a strong interest in determining the value of the muon lifetime to higher and higher precision using more sophisticated experiments and analysis. Additionally, the muon lifetime is a relevant quantity for physics education as the cosmic muon flux allows it to be measured with equipment that is common to undergraduate laboratories. The methods used in these investigations follow the same basic principle: producing muons from a source, stopping them in a target, then measuring the time difference between the stopping time and the decay time. A fit is then applied to the resulting histogram of the form $N(t) = Ne^{\lambda t} + C$, where N, λ and C are parameters to be fit corresponding to the normalisation, rate parameter and constant background respectively. As muon decay times are exponentially distributed, the time between stopping and decay will have the same rate parameter as the time between muon production and decay and hence the muon lifetime value for the experiment is given by $\tau_\mu = \frac{1}{\lambda}$.

In precision muon experiments, the main focus of experimental design is to account for sources of noise, which include detection of ionising radiation, noise within the scintillator, electrons/positrons from muons decaying before reaching the target, and muon spin precession. All precision experiments use beams of antimuons to ensure the rate parameter of the decay is not modified by muon capture. The flux of e^+ from μ^+ decaying before reaching the target may be reduced through use of velocity selecting magnetic and electric fields, as is done in the MuLan experiment [18]. Spin precession of muons and the weak interactions ability to violate parity causes causes the angular distribution of the positrons produced in muon decay to be a asymmetrically distributed. To account for this, detectors in these precision experiments aim to cover as close to a solid angle 4π sr as possible. The MuLan experiment achieves this through use of a positron detector made of 170 triangular scintillator pairs arranged in a 'soccer ball' shape [19] which covers approximately

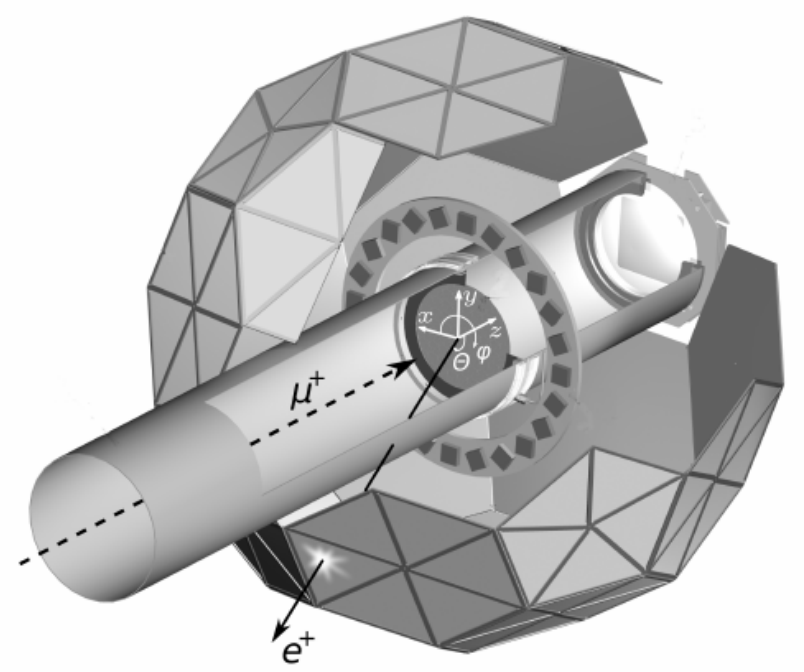

Figure 2: Sketch of the experimental setup used in the MuLan experiment adapted from [20].

70% of the full sphere depicted in Figure 2.

Educational setups are comparatively far less complicated, allowing them to be more accessible and easily understandable. Use of the cosmic muon flux as the source removes the need for a particle accelerator, with the added advantage of meaning the experiment requires no additional harmful radiation dose to participants. The detectors used in these experiments are commonly composed of a scintillator (often plastic) connected to a photomultiplier tube (PMT), which sends signals to a discriminator and then further to a processor (either on an external computer or inbuilt). When muons enter the scintillator, photons are produced which will enter the photomultiplier tube (PMT) and produce a signal. If the muon then stops in the scintillator, the resulting electron will produce further photons and an additional signal. These signals pass through the discriminator, which determines if the signal strength lies above a given threshold and if so passes the signals to the processor for analysis. The detector this project focuses on is the TeachSpin muon physics apparatus [7], [21]. This setup comprises of a 12.7cm tall, 15.2cm diameter cylindrical polyvinyl-toluene (PVT) scintillator connected to a 5.1cm 10-stage bi-alkali (Sb-Rb-Cs and Sb-K-Cs) PMT. These components are wrapped in aluminium foil to prevent light leaks and the setup is enclosed within a 36cm tall, 15.2cm diameter aluminium tube capped at both ends to protect the detector.

Additionally, an LED is installed near to the scintillator to allow detections to be simulated. A sketch of this setup can be seen in Figure 3. This setup measures lifetimes via use of an inbuilt timeout system. When a particle is detected, a timer begins counting cycles of the inbuilt clock. This timer will stop either when a second particle detection is made before a predetermined 'time-out' time of 20μs, or when the clock reaches the timeout time. The measured muon decay time is then taken to be the time between the two detections measured by the inbuilt clock. After a successful measurement, the detector resets and no detections may be made for 1ms.

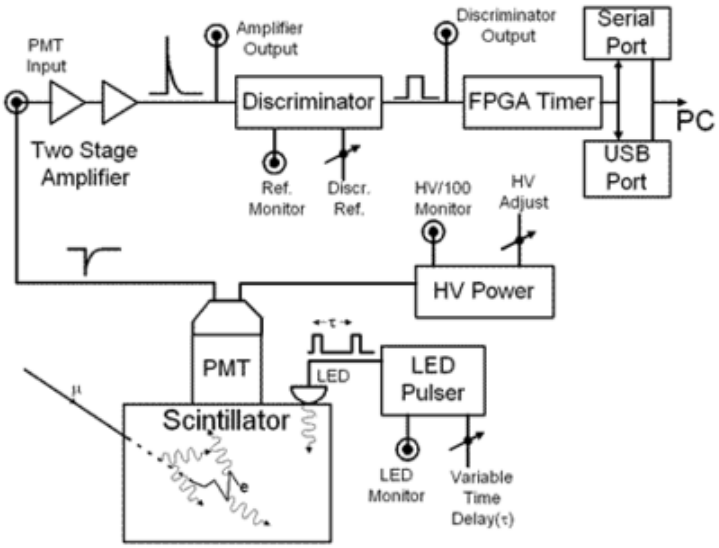

Figure 3: A sketch showing the components of the TeachSpin muon physics apparatus produced by [21].

As the cosmic muon flux is composed of both μ^+ and μ^-, the effects of muon capture must be accounted for in data analysis. The most precise way to do this is to fit the data to the sum of two exponential distributions with differing rate parameters:

$$N(t) = N_1 e^{\lambda_1 t} + N_2 e^{\lambda_2 t} + C \tag{4}$$

where the greater of λ_1 and λ_2 is the measured value of the effective μ^- decay rate λ_- and the lesser is the μ^+ decay rate λ_+, N_1 and N_2 are the corresponding numbers of decaying $mu^{\pm}$ detected and C is the background rate. These parameters may then be compared to known values of the muon lifetime ($\lambda_+ = 1/\tau_+$) and the effective μ^- decay rate in matter ($\lambda_- = \lambda_+ + \lambda_c$). However, due to the low value of the muon flux at sea level, collecting enough measurements to be able to resolve the values of λ_+ and λ_- may take many days of measurement, which may not be feasible

for educational experiments with limited laboratory time. A less data intensive alternative is to fit the data with a single exponential distribution:

$$N(t) = Ne^{-\lambda_{avg}t} + C \tag{5}$$

where the rate parameter is given by:

$$\lambda_{avg} = \lambda_+ + \lambda_c/(\rho + 1) \tag{6}$$

ρ is the charge ratio of cosmic muons, N is the total number of detected decays and C is again the rate of background detections. This distribution may be derived from Equation 4 using first-order Taylor expansion of the exponential ($e^{-\lambda t} \approx 1 - \lambda t$), making it only approximate and therefore limiting the accuracy of results that may be obtained. This is acceptable for educational setups, as the precision of these experiments is low enough that this is unlikely to affect results.

2.3 Monte Carlo simulations

In a scientific context, the term Monte Carlo (MC) refers to computational algorithms and mathematical methods which use random numbers to produce results. This definition is extremely wide, making the field of MC a very general one. Within HEP MC techniques are used for both theoretical calculations and for simulations of detector setups, the second of which is the focus of this project. Two of the most common MC software packages used for detector simulations are GEANT4 [22] and FLUKA [23], which have been used for simulation of a wide range of scientific setups including radiotherapy and space telescopes [24]. When simulating the cosmic muon flux, these packages are often used in conjunction with MC packages which simulate the air showers produced by cosmic rays such as CORSIKA [25] or COSMOS [26]. Applications of these simulations include identification of background sources in neutrino experiments [27] and the simulation of educational detector setups [28]. While bespoke MC simulators of the cosmic muon flux are rare due to the success of GEANT4 and FLUKA, a small number do exist. A prominent example is CMSCGEN - a standalone MC generator created for the CMS collaboration for data analysis of test detections of cosmic muons [29].

This project focuses upon building an open standalone detector simulation using Python. In order to achieve this, two common MC sampling techniques have been applied: the inverse transform

method, and acceptance-rejection sampling. These techniques are described in detail in [10], and will be briefly introduced here. Use of these techniques allowed sampling of the distributions of the cosmic muon flux described in subsection 2.1 using the pseudo-random number generator Python module random [30], which was used as the source of uniformly distributed random variables. The inverse transform method is the preferred method for sampling variables of the two, as it is both simpler and more efficient. The steps of applying this method to sample a given continuous probability density function (P.D.F.) $f(x)$ are as follows:

1. Obtain the cumulative distribution function (C.D.F.) $F(a) = P(x \leq a) = \int_{-\infty}^{a} f(x)dx$.
2. Calculate the inverse function of the C.D.F. $F^{-1}(p) = a$ where $p = P(x \leq a)$.
3. Generate a uniformly distributed random variable u.
4. Calculate $X = F^{-1}(u)$ - this is the output, and will have the distribution described by $f(x)$.

This method may be applied to any distribution for which the inverse C.D.F. is obtainable, for example the exponential distribution $f(x) = \frac{1}{\tau}e^{-x/\tau}$ which has an inverse C.D.F. of $F^{-1}(p) = -\tau \ln(1-p)$ and is sampled in this project to produce muon lifetimes and production times. Despite the relative simplicity of this method, obtaining the inverse C.D.F. of a distribution is not always possible. When this was the case, the inverse-transform method - a method which is applicable to any distribution with a known P.D.F. - was used in its place. In order to sample a P.D.F. $f(x)$ this method follows the following steps:

1. Choose a candidate function $Cg(x)$, where $g(x)$ is a normalised easily sampled P.D.F. and C is a scaling constant such that $Cg(x) \geq f(x)$ for all x.
2. Generate a candidate value of x (x_c) which has the distribution described by $g(x)$, along with a value u uniformly distributed between 0 and 1.
3. Compare the values $uCh(x_c)$ and $f(x_c)$: If $uCh(x_c) \leq f(x_c)$, accept x_c as the output. Otherwise, reject x_c and repeat from item 2 until a value is accepted.

The efficiency of this method is given by $1/C$, which is maximised when $C = 1$ - i.e., the method is most efficient when $g(x)$ is as similar as possible to $f(x)$. In order to produce efficient code, sensible candidate functions which describe the target P.D.F. well must be obtained.

3 Methodology

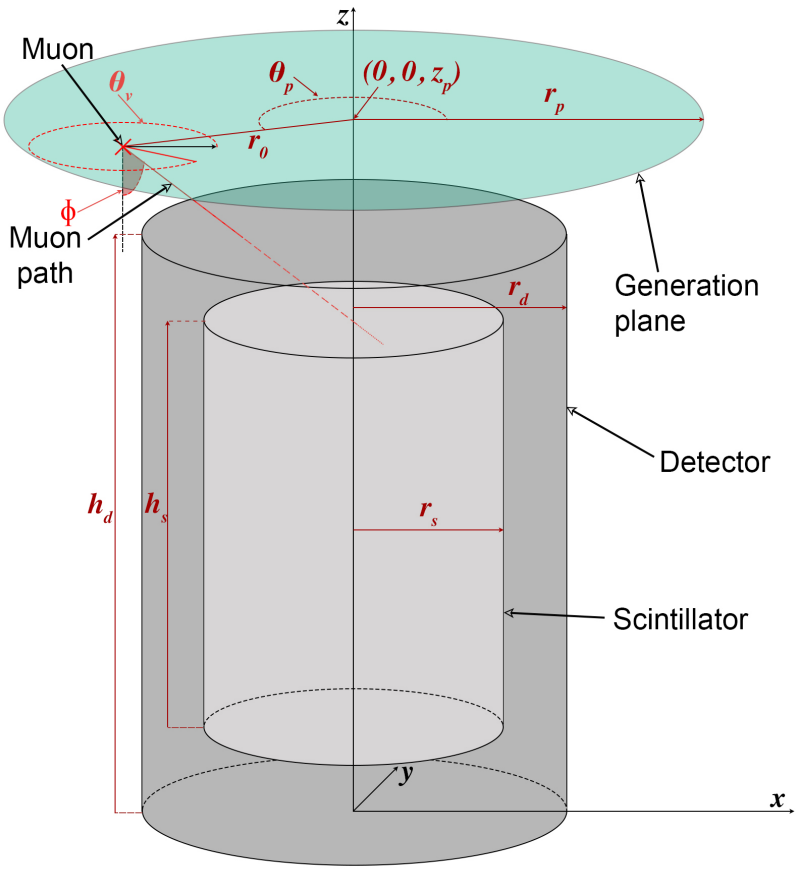

Figure 4: A sketch of a system with a single detector of height h_d and radius r_d positioned at $(0, 0, 0)$ containing a scintillator of radius r_s and height h_s. The muon plane lies above the detector at $(0, 0, z_p)$ and has radius r_p. A muon generated with an initial position in cylindrical coordinates of (r_0, θ_p, z_p) is also shown. The muon's path is defined by its azimuth angle θ_v and zenith angle ϕ.

In order to simulate the educational muon lifetime experiment the system was divided into three main objects: a muon plane (also referred to as a 'generation plane'), which holds the properties and limits of the simulated portion of cosmic muon flux; muons, instances of which hold the properties of each muon in the simulation; and the detector, instances of which contain the position, geometry, material properties and detection data of each detector. These objects interact via class methods discussed subsection 3.1 and subsection 3.2. A fourth object, the system, was created to streamline the interaction of these objects during a simulation and provide simple methods for data analysis

and presentation and is discussed in subsection 3.3. A sketch of a system containing a single detector positioned at (0,0,0) is shown in Figure 4. The accuracy and efficiency of these methods has been tested through several investigations described in subsection 3.4.

3.1 Muons

Within the simulation, muons are specified by the following properties: lifetime τ, kinetic energy E, velocity v, Lorentz factor $\gamma = 1/\sqrt{1 - v^2/c^2}$, zenith angle of velocity ϕ, azimuth angle of velocity θ_v, path length l, position in cylindrical coordinates (r, θ_p, z), and the time of generation t_g. The lifetime, momentum, velocity angles, position and generation time are randomly generated using either the inverse transform method or the acceptance-rejection method. Kinetic energy, velocity and Lorentz factor are calculated from the momentum p using the relations $p = \gamma mv$ and $E = (\gamma - 1)mc^2$. The methods used for generating each of these properties are summarised in Table 1. It should be noted that while the method for generating p is listed here as it is relevant for the generation of E, v and γ, momentum is not saved as a property of muons due to the redundancy of storing both p and v. For this project, Equation 2 was parameterised using data from Durham, UK due to its proximity to London, where the simulation is assumed to take place. These parameter values are $I_0 = 72.5 \pm 0.2\text{m}^{-2}\text{s}^{-1}\text{sr}^{-1}$, $n = 3.06 \pm 0.03$, $E_0 = (3.87 \pm 0.07) \times 10^3\text{MeV}$, and ϵ is fixed at $\epsilon = 854$. These parameter values were obtained through measurement of muons with momentum greater than 500MeV/c and hence the distribution's validity for momenta below this point is unknown.

The muon plane object stores the limits of muon initial position and energy, P_μ, the last produced value of t_g and the rate of muon production. The rate of muon production is calculated through integration of Equation 2 between the specified minimum and maximum muon momenta. This value is then multiplied by the proportion of detectable zenith angles, $\frac{1}{\pi}(\sin(2\phi) + 2\phi)$, where $\phi_{max} = \tan^{-1} \frac{r_p + r_s}{h_p - (h_s + h_{sp}}$ which is calculated for all detectors and taken to be the maximum value. Muons are generated through the muon plane method *muon_plane.gen_muon*, which creates a new instance of the *muon* class and assigns its value of t_g by sampling Δt and adding this value to the previous t_g. There are two methods for creating instances of the *muon* class: by sampling the properties of the muon at the time of generation, or taking the values from a pre-generated list of property values. Pre-generated values are obtained using the muon plane method

Symbol	Range	Sampling method	P.D.F./Equation
τ	$0 < \tau < \infty$	Inverse transform	$P(\tau = x) = \frac{1}{\tau_\pm} e^{-x/\tau_\pm}$
$\tau_\pm$	$\tau_\pm = \tau_-$ or $\tau_\pm = \tau_+$	Uniform sampling	$P(\tau_\pm = \tau_-) = P_\mu, P(\tau_\pm = \tau_+) = 1 - P_\mu$
p	$p_{min} \leq p \leq p_{max}$	Acceptance-rejection	$P(p = x) = N(E_0 + x)^{-n}(1 + x/\epsilon)^{-1}$
γ	$1 \leq \gamma < \infty$	Calculated from p	$\gamma = \sqrt{1 + p^2/(m^2c^2)}$
v	$0 \leq v < c$	Calculated from γ	$v = c\sqrt{1 - 1/\gamma^2}$
E	$0 \leq E < \infty$	Calculated from γ	$E = (\gamma - 1)mc^2$
ϕ	$0 \leq \phi \leq \pi/2$	Acceptance-rejection	$P(\phi = x) = \frac{4}{\pi}\cos^2(x)$
θ_v	$0 \leq \theta_v \leq 2\pi$	Uniform sampling	$P(\theta_v = x) = \frac{1}{2\pi}$
r_0	$0 \leq r_0 \leq r_p$	Inverse transform	$P(r_0 = x) = 2x/r_p^2$
θ_p	$0 \leq \theta_p \leq 2\pi$	Uniform sampling	$P(\theta_p = x) = \frac{1}{2\pi}$
t_g	$t_g(i-1) < t_g(i) < \infty$	Inverse transform	$t_g(i) = t_g(i-1) + \Delta t$, $P(\Delta t = x) = (\pi r_p^2/60)e^{-x\pi r_p^2/60}$

Table 1: The properties of muon in the simulation along with their methods of generation. The first generation time $t_g(0) = 0$

muon_plane.pre_generate, which is run once when the plane is initialised and again whenever all stored values have been used. Pre-generation is advantageous as it allows values to be generated in parallel through use of the high-performance computing Python module Numba [31], which is capable of improving the performance of the simulation. Generating muons upon a plane above the detector has the disadvantage of not being able to simulate detection of horizontally travelling muons, however this was taken to be acceptable for two reasons. Firstly, the correlation of muon momentum and zenith angle means that high-zenith muons are more likely to have energies that do not allow them to stop within the detector. While this correlation has not been implemented in the simulation, omission of these angles may be used to approximate of this effect. Secondly, horizontally travelling muons have a low flux due to the $\cos^2$ distribution of the muon's zenith angle. The combination of these two effects means that omission of high-zenith muons is unlikely to have a large effect upon the simulations results.

muon.detectable tests if a muon may be detected by a detector in the system given its path, energy, lifetime and initial position. This method returns the detection times if detected and

optionally returns counts of how many muons were rejected for each reason. Firstly, the muon's initial position and approach angles are considered to determine if its path coincides with a scintillator, assuming the muon has a perfectly straight path. This is done by using the following equations for the muon's radial position at a given height ($r(z)$) and vice-versa ($z(r)$):

$$r(z) = \sqrt{r_{\mu d}^2 + (z_{\mu d} - z)\tan\phi[(z_{\mu d} - z)\tan\phi - 2r_{\mu d}\cos(\pi - \theta_{\mu d} + \theta_v)]} \tag{7}$$

$$z(r) = z_{\mu d} - \frac{1}{\tan\phi}[r_{\mu d}\cos(\pi - \theta_{\mu d} - \sqrt{r^2 - r_{\mu d}^2\sin^2(\pi - \theta_{\mu d} + \theta_v)}] \tag{8}$$

If $z_{sb} < z(r_s) \leq z_{st}$ (where z_{sb} and z_{st} are the z coorindate of the bottom and top of the scintillator respectively) the muon enters the scintillator from the side. If $0 \leq r(z_{st}) \leq r_s$, the muon enters the scintillator from the top. If either check is passed, the distances along the muons path from the initial position to the detector and scintillator entry points (l_d and l_s) are calculated using $l_{d/s} = (z_{\mu d} - z(entry))/\cos\phi$, where $z(entry) = z(r_d$ for the detector and $z(entry) = z(r_s$ for the detector) if the muon enters from the side, or $z(entry) = z_{st}$ or $z(entry) = z_{sd}$ if the muon enters from the top, z_{sd} being the height of the top of the detector. If this check is passed, the muon's energy and lifetime are tested through *muon.propagate*, which simulates the energy loss of the muon as it passes through the detector.

muon.propagate splits the path of the muon into three sections: from production to the detector (path length l_d), where the muon travels through air; from the entry point of the detector to the scintillator (path length $l_{sp} = l_s - l_d$), where the muon travels through the detector's aluminium casing and air; and the distance within the scintillator in which the muon travels through PVT. The relevant properties of these material are shown in Table 2.

Energy loss within the air is assumed to be small and hence the approximation that muons lose energy at a constant rate given by $-\langle dE/dx\rangle \approx 2$ MeVg^{-1}cm$^2 \equiv S_0$ is valid here [1] is used for the first section. This is valid as the energy lost per distance travelled is given by $\rho \times -\langle dE/dx\rangle$ and the density of air is low. Application of this approximation follows the process outlined in [7]. Firstly, the value of γ at the start (γ_1) and end (γ_2) of this section are calculated by subtracting the energy loss from the muon's energy and recalculating γ. The increase in the muon's rest frame

Material	<Z/A>	ρ (gcm^{-3})	I (MeV)	a	x_0	x_1	$\bar{C}$	δ_0
Air	0.49919	1.204×10^{-3}	8.57×10^{-5}	0.10914	1.7418	4.2759	10.5961	0.0
Aluminium	0.48180	2.699	1.66×10^{-4}	0.08024	0.1708	3.0127	4.2395	0.12
PVT	0.54141	1.032	6.47×10^{-5}	0.16101	2.4855	0.1464	3.1997	0.0

Table 2: Properties of the materials present in the simulation relevant to energy loss, obtained from [10].

clock t_μ while propagating this distance is then calculated using the following equation:

$$\Delta t_\mu = \frac{mc}{\rho S_0} \int_{\gamma 2}^{\gamma 1} \frac{1}{\sqrt{\gamma^2 - 1}} d\gamma = \frac{mc}{\rho S_0} \ln \left[\frac{\sqrt{\gamma_1^2 - 1} + \gamma_1}{\sqrt{\gamma_2^2 - 1} + \gamma_2} \right] \tag{9}$$

The change in the detector's rest frame clock t_d may then be calculated using $\Delta t_d = (\gamma_1 + \gamma_2) t_\mu / 2$, where the midpoint of γ_1 and γ_2 has been taken as the equivalent Lorentz factor for this distance as $\gamma_1 \approx \gamma_2$ as the energy change is small. After this point, the density of the considered materials is no longer small enough for the constant energy loss approximation to be valid so a more detailed approach is required. Within the detector casing, the Bethe-Bloch equation is applied iteratively to the muon. Firstly, in the distance from detector entry to scintillator entry the equation is applied in 3 steps of distance $dl = l_{sp}/3$. This small number of iterations is acceptable as the distance between the casing and the scintillator is relatively small, and the material here is air therefore the energy changes for each of these iterations are low. For iterations where the sum of these distances is less than 0.1cm the material properties of aluminium are used, and after the properties of air are used. If $dl > 0.1$cm, 1 iteration is applied with distance 0.1 and 2 iterations of distance $dl = (l_{sp} - 0.1)/2$ are applied using air's properties. The time for the muon to traverse this distance in the detector's rest frame is given by $\Delta t_d = dl/v$, and the time elapsed in the muon's rest frame is $\Delta t_\mu = dl/(\gamma v)$, where γ is the Lorentz factor before energy loss is applied. If at any point the energy change is greater than the muon's current energy or $t_\mu > \tau$, the muon is rejected. If this check is passed, the muon enters the scintillator. The energy loss after this point is performed in 100 iterations of the Bethe-Bloch formula (or less, if the muon stops within the scintillator). In each of these iterations the muon's rest frame clock is increased by $\Delta t_\mu = (\tau - t_\mu(\text{scint. entry}))$, where t_μ(scint. entry) is the value of the muon's clock when it enters the scintillator, and the clock

in the detector frame is increased by $\Delta t_d = \gamma \Delta t_\mu$. The use of time-stepping avoids errors produced by distance-stepping when the muon's velocity approaches 0 and the time taken to traverse a set distance may diverge. The distance travelled in each iteration is calculated using $ds = \gamma \Delta t_\mu v$, the sum of which may be used to calculate the total path length. If the energy change for an iteration exceeds the muon's energy, the muon stops within the scintillator and its time of decay in the detector is given by $t_d + \tau - t_\mu$, as the muon's rest frame is now the detector's rest frame. Once the muon decays (either by stopping or undergoing all 100 iterations of energy loss), its position is checked to determine if it is still within the scintillator. The final position of the muon is given by $l\hat{\mathbf{v}} + \mathbf{x_0}$, where l is the total path length, $\hat{\mathbf{v}}$ is the unit vector in the direction of the muon's velocity and $\mathbf{x_0}$ is the muon's initial position. The distance in the $x - y$ plane between this point and the centre of the detector is then determined. If this distance is less than the radius of the scintillator and the z coordinate is greater than the z of the scintillator's base, the muon has stopped within the scintillator; otherwise it has passed through before decaying and is rejected. If all checks are passed, the times of scintillator entry and muon decay are returned as the final output from both *muon.propagate* and *muon.detectable*.

3.2 Detectors

The detector object stores the material properties and dimensions of the detector and scintillator along with detector timeout and reset times. Additionally, detectors store lists of the times at which detections were made, which may be analysed to produce the values of measured muon lifetimes as well as lists of initial muon energies and path lengths. Material properties, dimensions, timeout time and reset time may be specified at object initialisation, allowing detectors to be almost fully customisable with the main limitation being that the detector's geometry is fixed to be an upright cylinder. The default material properties of the detector and scintillator are aluminium and PVT respectively, with the specific values used shown in Table 2. Default dimensions are given by the TeachSpin detector dimensions ($r_d = r_s = 7.6$cm, $h_d = 36.0$cm, $h_s = 12.7$cm [21]), and default timeout and reset times are 20μs and 1ms respectively. As more than one detector may be present in the simulation at once, detectors require a position, specified in Cartesian coordinates. Overlapping detectors are not permitted, and produce an error during system initialisation.

The detector has 3 main methods: *detector.muon_detection*, *detector.add_noise*, and *detector.measure_lifetimes*, which handle muon detections, background events and the lifetime measurement system respectively. *detector.muon_detection* takes the scintillator entry and decay times output by *muon.detectable* and appends them to the list of detection times. Additionally, the initial energy of the muon and the muon itself are taken as inputs, allowing the energy and path length to be recorded for inspection later.

detector.add_noise adds data to the detector's list of detection times which does not follow the muon lifetime distribution. This is done by providing either a list of rates $(\lambda_1, \lambda_2, ...)$ in units of s^{-1} or a total number of events (N) to be added. Background sources are assumed to produce events according to a exponential distributions with rate parameter λ_i or N/t_{max}, where t_{max} is the time of the final detection made by the detector. The times between these events Δt_n are generated using the inverse transform method, with the time of the n^{th} event given by $t_n = \sum_{i=0}^{n} \Delta t_i$ where t_0 is the time of the first muon detection. Generated times are appended to the list of muon detection times.

After all detections have been made and noise has been added, *detector.measure_lifetimes* may be used to determine how the detector interprets the detections it has into lifetime measurements. Firstly, the list of detection times is sorted to ensure background detections, which are generated after muon detections, are properly treated. Next the list is iterated over, and the difference between the current event time and the next $(t_{i+1} - t_i)$ is determined. If this interval is found to be less than the timeout time of the detector it is recorded as a measurement. After a measurement is recorded any detections that occur within the reset time Δt_{reset} (i.e., between t_{i+1} and $t_{i+1} + \Delta t_{reset}$) are disregarded. When the loop reaches the final detection time (for which no interval is defined as the next time does not exist), the list of recorded time intervals is returned.

3.3 Systems

After the muon plane and any detectors have been created, the system may be initialised by creating a new system object and providing the plane and detectors as inputs. The detectors and muon plane are assigned as a properties of the system and the overlap of objects is then considered. If the horizontal distance between two detector positions is less than the sum of their two radii

and the z coordinate of one detector is not greater than the height of the other, they overlap and an error is raised. Additionally, if the muon plane's height is less than the sum of a detector's z coordinate and its height, the detector overlaps with or lies above the plane and a corresponding error is raised.

After successful initialisation, the simulation may be run with the *system.simulate*, which produces a specified number of muon detections. Additional optional parameters allow the level of detail of the simulation to be specified: the Boolean *keep_passing_mu* controls whether the scintillator entry time of muons entering the detector are kept or disregarded, which can provide a source of background noise particularly if large energy ranges are chosen to be simulated. Similarly, the Boolean *treat_casing* controls whether the aluminium casing of the detector should be considered: if false, the detector will be treated as simply a plastic scintillator, which can accelerate the simulation at the cost of some physical accuracy. *use_pre_gen* may be set to true to allow pre-generated muon properties to be used throughout the simulation, and *n_pre_gen* specifies the number of pre-generated muons to create per iteration. Noise can be added to the simulation through the *noise_rates* and *noise_total* variables which correspond to the inputs of *detector.gen_noise*. The *track_rejections* input may be set to true to make the method return an additional dictionary containing the number of muons rejected by each method (path not coinciding with the scintillator, decaying before the scintillator, stopping in the air, stopping in the aluminium casing, stopping in the air between the casing and the scintillator, or passing through the scintillator). Finally, the *prog_bar* Boolean will show a progress bar displaying how many muons have been detected and an estimation of the time remaining for the simulation if set to true.

During *system.simulate*, muons are generated from the generation plane until one is determined to be detectable by *muon.detectable*. When this happens, the muon's properties are recorded via *detector.muon_detection*. This process is done until the requested number of muons have been detected, at which point the output dictionary is assembled. This dictionary stores the lifetime, path length and energy measurements of the i^{th} detector in the entries with keys 'lifetime i', 'path_len i' and 'energies i'. The output and rejections dictionaries are saved as a property of the system and additionally returned.

After running *system.simulate* to gather data, the other system methods may be used for data analysis and presentation. *system.one_t_fit* and *system.two_t_fit* apply the fits described in

Equation 5 and Equation 4 respectively using the SciPy module's [32] *curve_fit* function. This performs a non-linear least squares fit for each of the respective equations to the histogrammed data to obtain both the optimal parameters and the standard deviation errors of the fit. The number of bins used in the fit histogram, which can limit the accuracy of results if too low, may be specified when these methods are used. A final optional parameter *which_det* allows a detector index to be specified, in which case only data from that particular detector will be analysed.

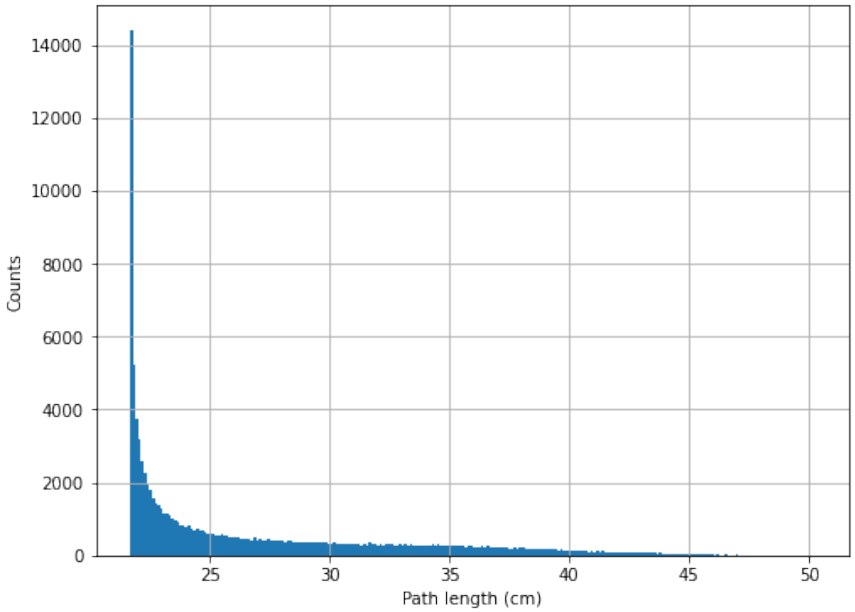

Figure 5: A histogram of measured muon path lengths created with 250 bins. Data was measured using a by a detector of default dimensions positioned at $(0, 0, 0)$ and muons generated by a muon plane with radius $5\times$ the detector radius and positioned 10cm above the detector. 100,000 detections were made, and the momentum limits used were 1 MeV$\leq p \leq$ 200 MeV.

The *system.obtain_metrics* method applies both of the fitting methods mentioned above to obtain the optimal parameters of each of the fit and use them to produce the final results of the experiment, which are stored in a dictionary for ease of access. Additionally, to investigate how the parameters of the simulation affect the detection rate, the proportion of generated muons that are detected and the number of lifetimes measured are determined. Uncertainties on the experiment results are calculated by propagating statistical errors from the fit parameters. The goodness of each fit is quantified by calculating the χ^2 test statistic and corresponding p-value using and the corresponding probability using the *scipy.stats.chisquare* function. The contents of this dictionary

are shown in Table 5 and the formulae used to calculate uncertainties are in Table 6, both of which may be found in Appendix B.

The final system method *system.plot_result* allows the measured lifetimes, energies or path length histograms to be plotted using a specified number of bins. Lifetime plots may be optionally accompanied by plots of each of the fits obtained using *system.one_t_fit* and *system.two_t_fit*. An example of a path length plot produced by this function is shown in Figure 5, while examples of lifetime and energy plots can be seen in Figure 6 and Figure 7 respectively.

3.4 Simulation assessment

The accuracy of the simulation was quantified by determining the most accurate values of the simulation metrics τ_{avg}, τ_+, τ_-, and ρ that could be produced, while ensuring that the energy lost by detected muons and the rate of detection were close to expected values. The efficiency was then assessed by determining how the time taken for the simulation to obtain these values. The most accurate values of the metrics were determined by running simulations with the number of muon detections ranging from 100 to 1,000,000 and observing the response of each metric. The efficiency of the simulation was inspected by timing the simulation of these results using the iPython magic command *%timeit* [33], which allowed the number of muon detections per real-time seconds to be obtained.

Tests were run using a system setup chosen to be as realistic as possible while also minimising the number of undetectable muons generated. For simplicity, only systems containing a single detector positioned at the origin of the system were used in analysis. The detector dimensions were kept to be consistent with the TeachSpin apparatus, allowing for comparison with previous experimental data. The muon plane radius and height were additionally kept constant, as these variables affect only the amount of energy lost by muons before entering the detector and the maximum detectable zenith angle. The first of these effects is made redundant by altering the momentum range muons are generated with, while the second was taken to be large enough that only muons with very high zenith angles are excluded. The plane height and radius used in the system setups was $h_p = h_d + 10 = 46$cm and $r_p = 5r_d = 38$cm, producing a maximum detectable zenith angle of $\phi_{max} = 1.1275 = 0.7178 \times \frac{\pi}{2}$, with a detectable proportion of the zenith distribution

being $\int_0^{\phi_{max}} \frac{4}{\pi} \cos^2 \phi d\phi = 0.964$.

The momentum range of muons was chosen such that it was consistent with previous simulations of similar detector setups, which found that muons deposit an average of 100MeV or less within their detectors [28] [34]. The geometry and materials used in these detectors differ from the TeachSpin setup, so these results are not directly comparable to our simulation however they give a good indication of the energy range of muons that should stop within the detector. A momentum range of 1-200MeV/c was chosen, corresponding to a kinetic energy range of approximately 0-120MeV. This likely over-estimates the muon kinetic energy range that should be detected, however this should be accounted for via the energy loss algorithm. This assumption was tested via further tests using momentum ranges of 1-175MeV/c, 1-250MeV/c, 1-500MeV/c and 1-1,000MeV/c with an otherwise identical system.

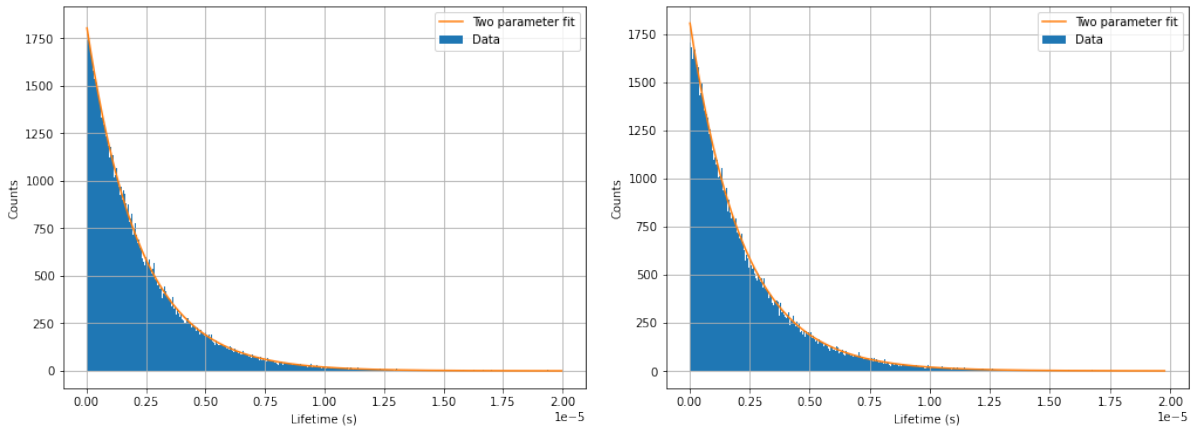

Figure 6: Comparison of lifetime histograms with *keep_passing_mu* set to true (left) and false (right). The corresponding values of τ_{avg} are $(2.205 \pm 0.007) \times 10^{-6}$ and $(2.200 \pm 0.009) \times 10^{-6}$ respectively, which differ by less than their experimental uncertainty.

Simulations were run using *treat_casing* set to be true, *keep_passing_mu* to be false, and the number of pre-generated events kept constant at 1,000,000. The number of bins used in the histograms for fits was varied to maximise the $P(\chi^2)$ value of each of the fits. For larger samples this was found to be impossible, due to known issues with the p-value of large samples [35]. The omission of passing muons was found to not affect the results via a further test using the above setup for 100,000 detections to determine what difference this made to results. A comparison between the lifetime histograms produced with this parameter set to true and false respectively can be seen in

Figure 6.

Additional tests were undertaken to determine the performance impacts and validity of the methods *detector.add_noise* and *muon_plane.pre_generate*. The first of these ran simulations with differing rates of background detections ($0.1s^{-1}$, $1s^{-1}$, $10s^{-1}$, and $100s^{-1}$), timing the production of results. The effect of pre-generation was tested by timing the production of 100,000 events using both pre-generation of 1,000,000 events, 10,000,000 events, and normal sampling. These simulations were run 4 times each to determine the average and best times possible for each method. All tests were run using the freely available Google Colaboratory [36], which provides access to an 2-core Intel Xeon CPU with a clock speed of 2.2GHz and 13GB of RAM.

4 Results

4.1 Simulation accuracy

The values obtained from the parameters of the fits for the simulation with 1,000,000 muon detections are presented in Tables 3 and 4. The variation of each of these values with the number of muon detections is shown in Appendix C.

	τ_{avg}	τ_{+est}
Obtained value	$(2.206 \pm 0.003) \times 10^{-6}$	$(2.220 \pm 0.003) \times 10^{-6}$
Expected value	2.183×10^{-6}	2.197×10^{-6}

Table 3: Values obtained from the single exponential fit made to the histogram of measured lifetimes for the test with 1,000,000 muon detections described in subsection 3.4, along with their expected values.

Despite the values of the lifetimes being correct to 2 significant figures, it is clear from inspection of the uncertainties that these values do not agree with the expected values suggesting a source of systematic error is present. Figures 10-15 back this up by showing that simulations with greater than 50,000 muon detections have little variation in each of the parameters, suggesting that past this point the parameter fits have converged upon their most accurate value and the deviation is

	τ_+	τ_-	ρ
Obtained value	$2.206 \times 10^{-6} \pm 0.14$	$2.206 \times 10^{-6} \pm 0.14$	$1.000 \pm 2.1 \times 10^{-5}$
Expected value	2.197×10^{-6}	2.17×10^{-6}	1.277

Table 4: Values obtained from the double exponential fit made to the histogram of measured lifetimes for the test with 1,000,000 muon detections described in subsection 3.4, along with their expected values.

not due to a lack of data. These results additionally show that the analysis is unable to resolve the differing values of the muon lifetimes using the double exponential fit, as the double parameter fit simply reproduces the single parameter fit by taking $\tau_+ = \tau_- = \tau_{avg}$ and $\rho = 1$. The fact that the uncertainty upon the lifetimes produced by this fit is 5 orders of magnitude greater than the obtained value further demonstrates the inability of fit to resolve these lifetimes.

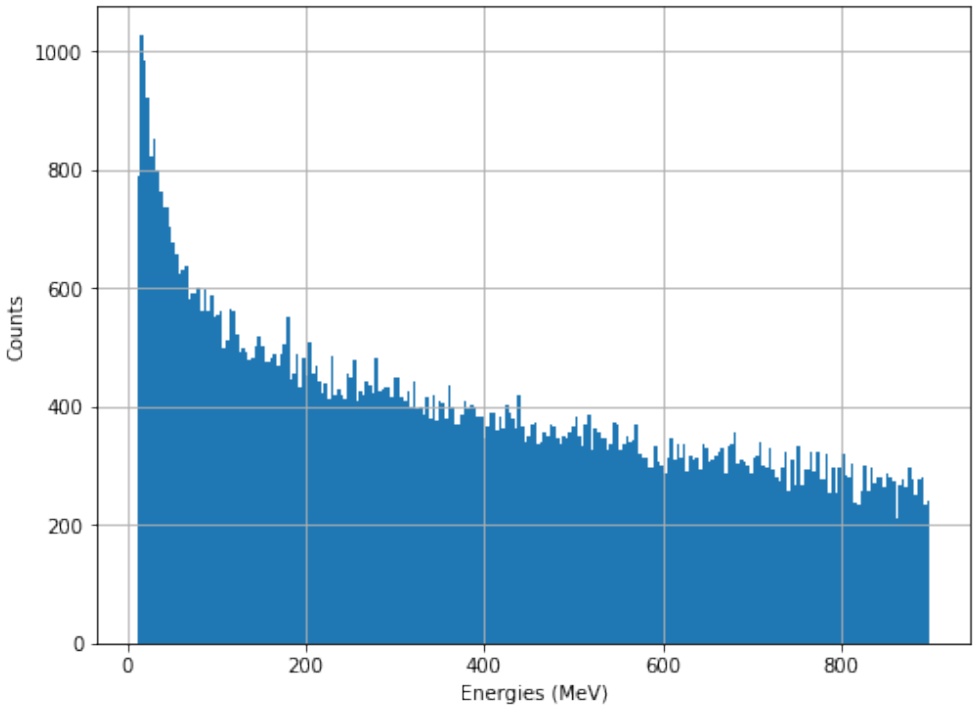

Figure 7: Histogram of the initial kinetic energies of detected muons in a test with muon momenta range of 1-1000MeV/c.

Variation of the momenta range muons may be generated with shows that the assumption that the energy loss algorithm accurately handles muon energy loss within the detector does not

hold. The histogram of initial kinetic energies of detected muons generated with a momentum range of 1-1000MeV/c shown in Figure 7 demonstrates that muons with all kinetic energies across the generated range are detected, despite the higher end of this range being far greater than the expected maximum energy that should be lost within the detector (100-200MeV). Figure 8 shows that there is a correlation between the upper limit of the muon momentum and the magnitude of the error in τ_{avg}, and the calculated Pearson coefficient of this correlation is 0.979, strongly suggesting the source of systematic error in the simulation results is the error in the energy loss algorithm *muon.propagate*. The likely reason for this is that the algorithm over-estimates the amount of energy lost within the scintillator. This would lead to muons with higher values of γ entering the scintillator and being brought to a stop when they should have passed through the scintillator. As their value of γ is greater than what is expected for low energy muons, the time between scintillator entry and decay for these muons will be increased leading to an increase in the produced average muon lifetime.

The average muon detection rate across all simulations with a momentum range of 1-200MeV/c was found to be $5.434 \pm 0.004\text{min}^{-1}$, which is approximately $5\times$ the expected value of 1min^{-1}. This value increases with the upper limit of muon momentum, which is to be expected as the rate of muon production is calculated via integration of the Equation 2 between the momentum limits. This disagreement with experiment is therefore another consequence of the error in the energy loss algorithm.

The tests of *detector.add_noise* show that the algorithm is working as expected, adding a constant value to all lifetime bins while still preserving the shape of the underlying exponential. This is shown best by the lifetime histogram for the test with a rate of 100 events s^{-1}, shown in Figure 9. The other rates tested were not large enough to produce a noticeable effect upon the distributions.

4.2 Simulation efficiency

The sum of times taken to complete the simulations while varying the number of detected muons was 6035s, producing a real time average rate of muon detection of $276 \pm 4\text{s}^{-1}$. This high rate allows the simulation to produce 100,000 detections, which is sufficient to produce the most accurate possible

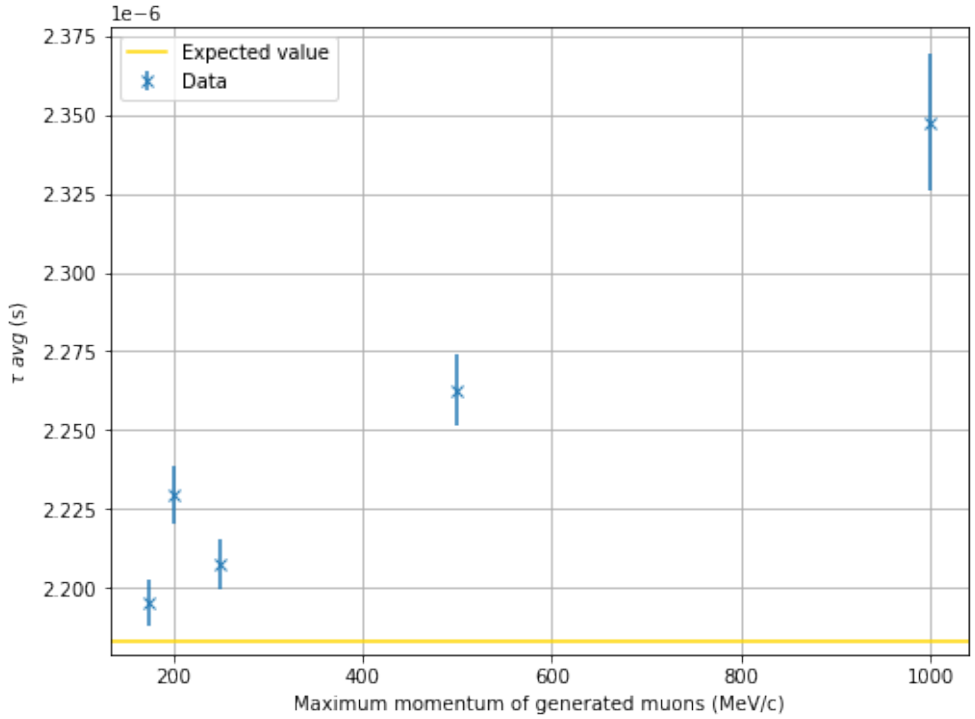

Figure 8: Variation of τ_{avg} with the upper limit of the muon momentum range. The minimum momentum was kept constant at 1MeV/c.

values from analysis, in 6 minutes of run time while production of 1,000,000 events takes roughly 1 hour. In comparison 100,000 detections would take an average of 69 days of real measurement with the expected detection rate of 1min^{-1}.

The time taken to produce results with the addition of background detections to the simulation shows that the *detector.add_noise* function adds a non-negligible amount of time to the simulation run time. Adding noise with a rate of 100s^{-1} to a simulation with 100,000 detections had an overall run time of 590s, which is 230s greater than the run made on an identical system with no added noise. The expected number of background events produced is 5.62×10^8 events, producing a mean real-time rate of noise generation of $(2.4637 \pm 0.0001) \times 10^6\text{s}^{-1}$.

The test of *muon_plane.pre_generate* showed that use of pre-generation is slightly slower than normal sampling, with the average times to produce each set of results being (340 ± 2)s for normally generated events and (345 ± 2)s for pre-generated events. The difference between these mean values is greater than the uncertainty upon the real time rate of generation, suggesting this difference

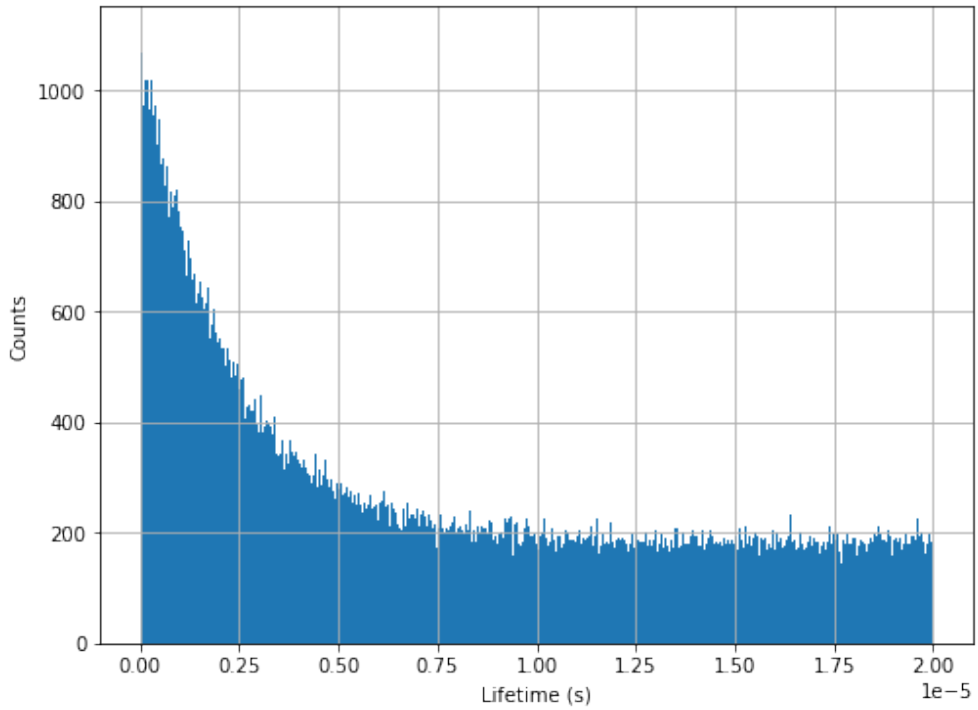

Figure 9: Lifetime histogram produced by a system with a background rate of 100 events s^{-1}.

is not due to random fluctuation. In theory, this method should be able to approximately halve the time taken to generate these values by taking advantage of the dual core processor used in these tests. This suggests that the generation of muon properties is not the rate determining step of the simulation, and that accelerating this process does not drastically increase the efficiency of the simulation. The most likely reason for the observed increase in run time is that the algorithm generates more events than are required. As an example, one of the iterations of this test generated a total of 4,057,564 muons. As the number of pre-generated events per use of *muon_plane.pre_generate* was set to 1,000,000, this required the plane to generate 5,000,000 events despite only using 57,564 events from the last iteration.

5 Conclusions and outlook

This project has produced a MC simulation which can efficiently simulate the results of an educational setup for measurement of the muon lifetime. Key features of the muon flux including the energy and angular distribution are simulated, along with the generation of generic background

detections. A set of analysis tools has been produced which allows for functional fits to be easily made to the collected data and the results of the simulation to be presented. However an error in the energy loss algorithm of the simulation causes muons to lose more energy than expected within the scintillator of the detector, producing a systematic error in the simulation results. While this may be accounted for by the user ensuring only muons within the detectable range of momentum (approximately 200MeV/c) are generated, this severely limits the accuracy of the simulation. The priority for future work is therefore producing a new energy loss algorithm which more accurately simulates the passage of muons through the scintillators of detectors. Further improvements may be made by implementing a better description of the muon flux at the low energies, as the validity of the current parameterisation is unknown in the detectable range of energies.

References

[1] T. K. Gaisser *et al.*, *Cosmic rays*. Cambridge: Cambridge University Press. DOI: 10.1017/CBO9781139192194.003.

[2] V. Hess, "On the Observations of the Penetrating Radiation during Seven Balloon Flights," *Phys. Zeitschrift 13*, pp. 1084–1091, arXiv: 1808.02927.

[3] S. H. Neddermeyer *et al.*, "Note on the nature of cosmic-ray particles," *Phys. Rev.*, no. 10, pp. 884–886, DOI: 10.1103/PhysRev.51.884.

[4] C. D. Anderson *et al.*, *Positrons from gamma-rays [4]*. DOI: 10.1103/PhysRev.43.1034.

[5] Y Fukuda *et al.*, "Evidence for oscillation of atmospheric neutrinos," *Phys. Rev. Lett.*, vol. 81, no. 8, pp. 1562–1567, 1998. DOI: 10.1103/PhysRevLett.81.1562. arXiv: 9807003 [hep-ex].

[6] S. N. Axani *et al.*, "The CosmicWatch Desktop Muon Detector: A self-contained, pocket sized particle detector," *J. Instrum.*, no. 3, P03019, DOI: 10.1088/1748-0221/13/03/P03019. arXiv: 1801.03029.

[7] T. Coan *et al.*, "A compact apparatus for muon lifetime measurement and time dilation demonstration in the undergraduate laboratory," *Am. J. Phys.*, no. 2, pp. 161–164, DOI: 10.1119/1.2135319. arXiv: 0502103 [physics].

[8] K. van Dam *et al.*, "The HiSPARC experiment," *Nucl. Instruments Methods Phys. Res. Sect. A Accel. Spectrometers, Detect. Assoc. Equip.*, vol. 959, p. 163 577, Apr. 2020. DOI: 10.1016/j.nima.2020.163577.

[9] R. Antolini *et al.*, "The EEE project," in *29th Int. Cosm. Ray Conf. ICRC 2005*, pp. 279–282. arXiv: 0607027 [physics].

[10] B. Abi *et al.*, "Measurement of the Positive Muon Anomalous Magnetic Moment to 0.46 ppm," *Phys. Rev. Lett.*, vol. 126, no. 14, Apr. 2021. DOI: 10.1103/PhysRevLett.126.141801. arXiv: 2104.03281.

[11] R. Carey *et al.*, "Mulan: a part-per-million measurement of the muon lifetime and determination of the Fermi constant," arXiv: 2108.09182.

[12] D. F. Measday, *The nuclear physics of muon capture*, 2001. DOI: 10.1016/S0370-1573(01)00012-6.

[13] Y. Abe *et al.*, "Muon capture on light isotopes measured with the Double Chooz detector," *Phys. Rev. C*, no. 5, p. 054 608, DOI: 10.1103/PhysRevC.93.054608.

[14] R. Ford, "SNOLAB: Review of the facility and experiments," in *AIP Conf. Proc.*, American Institute of PhysicsAIP, pp. 521–524. DOI: 10.1063/1.3700605.

[15] P. A. Zyla *et al.*, *Review of particle physics*. DOI: 10.1093/ptep/ptaa104.

[16] V. Khachatryan *et al.*, "Measurement of the charge ratio of atmospheric muons with the CMS detector," *Phys. Lett. Sect. B Nucl. Elem. Part. High-Energy Phys.*, no. 2, pp. 83–104, DOI: 10.1016/j.physletb.2010.07.033. arXiv: 1005.5332.

[17] P. Shukla *et al.*, "Energy and angular distributions of atmospheric muons at the Earth," *Int. J. Mod. Phys. A*, no. 30, DOI: 10.1142/S0217751X18501750. arXiv: 1606.06907.

[18] P. T. Debevec, "Improved measurement of the muon lifetime and determination of the Fermi constant," in *Proc. 6th Int. Work. CKM Unitarity Triangle, CKM 2010*. arXiv: 1108.4033.

[19] V Tishchenko *et al.*, "Detailed report of the MuLan measurement of the positive muon lifetime and determination of the Fermi constant," *Phys. Rev. D - Part. Fields, Gravit. Cosmol.*, vol. 87, no. 5, 2013. DOI: 10.1103/PhysRevD.87.052003. arXiv: 1211.0960.

[20] V. Tishchenko *et al.*, "Data acquisition system for the MuLan muon lifetime experiment," *Nucl. Instruments Methods Phys. Res. Sect. A Accel. Spectrometers, Detect. Assoc. Equip.*, vol. 592, no. 1-2, pp. 114–122, Jul. 2008. DOI: 10.1016/j.nima.2008.03.121.

[21] TeachSpin Inc., *Muon Physics | TeachSpin*. [Online]. Available: https://www.teachspin.com/muon-physics (visited on 10/30/2021).

[22] S. Agostinelli *et al.*, "GEANT4 - A simulation toolkit," *Nucl. Instruments Methods Phys. Res. Sect. A Accel. Spectrometers, Detect. Assoc. Equip.*, vol. 506, no. 3, pp. 250–303, Jul. 2003. DOI: 10.1016/S0168-9002(03)01368-8.

[23] G. Battistoni *et al.*, "The FLUKA code: Description and benchmarking," in *AIP Conf. Proc.*, American Institute of PhysicsAIP, pp. 31–49. DOI: 10.1063/1.2720455.

[24] J Allison *et al.*, "Geant4 developments and applications," *IEEE Trans. Nucl. Sci.*, vol. 53, no. 1, pp. 270–278, 2006. DOI: 10.1109/TNS.2006.869826.

[25] D Heck *et al.*, "CORSIKA: A Monte Carlo Code to Simulate Extensive Air Showers," *Forschungszentrum Karlsruhe*, pp. 1–90,

[26] K. Kasahara, *COSMOS Homepage*, 2014. [Online]. Available: https://cosmos.n.kanagawa-u.ac.jp/cosmosHome/index.html{\#}doc (visited on 03/02/2022).

[27] G. Bellini *et al.*, "Cosmogenic backgrounds in borexino at 3800 m water-equivalent depth," *J. Cosmol. Astropart. Phys.*, no. 8, p. 049, DOI: 10.1088/1475-7516/2013/08/049. arXiv: 1304.7381.

[28] F. Riggi *et al.*, "Muon decay: An old, yet alive experiment in the university physics curriculum," *Eur. J. Phys.*, no. 4, p. 045 702, DOI: 10.1088/0143-0807/37/4/045702.

[29] P. Biallass *et al.*, "Simulation of Cosmic Muons and Comparison with Data from the Cosmic Challenge using Drift Tube Chambers," CERN, Geneva, Tech. Rep.

[30] *random — Generate pseudo-random numbers — Python 3.10.2 documentation.* [Online]. Available: https://docs.python.org/3/library/random.html (visited on 03/15/2022).

[31] Anaconda, *Numba: A High Performance Python Compiler*, 2018. [Online]. Available: https://numba.pydata.org/https://numba.pydata.org/{\%}0Ahttp://numba.pydata.org/ (visited on 01/11/2022).

[32] P. Virtanen *et al.*, "SciPy 1.0: fundamental algorithms for scientific computing in Python," *Nat. Methods*, no. 3, pp. 261–272, DOI: 10.1038/s41592-019-0686-2. arXiv: 1907.10121.

[33] F. Pérez *et al.*, "IPython: A system for interactive scientific computing," *Comput. Sci. Eng.*, no. 3, pp. 21–29, DOI: 10.1109/MCSE.2007.53.

[34] P. S. Canflanca, "Monte Carlo Simulation of a Detector for Cosmic Rays," Ph.D. dissertation, University of Münster, 2014. [Online]. Available: https://www.uni-muenster.de/imperia/md/content/physik{_}kp/agwessels/thesis{_}db/ag{_}wessels/canflanca{_}2014{_}bachelor.pdf.

[35] M. Lin *et al.*, "Too big to fail: Large samples and the p-value problem," *Inf. Syst. Res.*, no. 4, pp. 906–917, DOI: 10.1287/isre.2013.0480.

[36] Google Colab, *Welcome to Colaboratory - Colaboratory*, 2020. [Online]. Available: https://colab.research.google.com/ (visited on 03/22/2022).

A Simulation code

All code used in this simulation is contained within the *Project Final.ipynb* available for download at the following url: `https://github.com/HugoNeely/MuonProject`.

B Simulation results

Value	Description	Formula
τ_{avg}	Inverse rate parameter of Equation 5	$\tau_{avg} = 1/\lambda_{avg}$
τ_{+est}	Estimated μ^+ lifetime from Equation 6	$\tau_{+est} = 1/(\lambda_{avg} - \frac{\lambda_c}{\rho+1})$
τ_+	μ^+ lifetime	$\tau_+ = 1/\lambda_1$
τ_-	Effective μ^- lifetime	$\tau_- = 1/\lambda_2$
ρ	Cosmic muon charge ratio	$\rho = N_1/N_2$
n_{gen}	Total number of muons generated	Tracked by *system.simulate*
n_{det}	Total number of muons detected	Specified by user
n_{meas}	Total number of decays measured	Length of lifetime arrays
χ_1^2	χ^2 parameter for the fit obtained from Equation 5	$\chi_1^2 = \sum \frac{(N_{obs}-N_{fit})^2}{N_{obs}}$
$P(\chi_1^2)$	p-value of χ_1^2	$P(\chi_1^2) = P(\chi^2 \geq \chi_1^2)$, d.o.f. = no. bins - 4
χ_2^2	χ^2 parameter for the fit obtained from Equation 4	$\chi_2^2 = \sum \frac{(N_{obs}-N_{fit})^2}{N_{obs}}$
$P(\chi_2^2)$	p-value of χ_2^2	$P(\chi_2^2) = P(\chi^2 \geq \chi_2^2)$, d.o.f. = no. bins - 6

Table 5: The results of the simulation obtained by *system.obtain_metrics*. For expediency it is assumed here that $\lambda_1 < \lambda_2$ and $N_1 > N_2$; in practice the greater of λ_1 and λ_2 is determined and used appropriately.

Value	Uncertainty formula
τ_{avg}	$\Delta\tau_{avg} = \tau_{avg} \times \Delta\lambda_{avg}/\lambda_{avg}$
τ_{+est}	$\Delta\tau_{+est} = \tau_{+est}$
τ_{+}	$\Delta\tau_{+} = \tau_{+} \times \Delta\lambda_{1}/\lambda_{1}$
τ_{-}	$\Delta\tau_{-} = \tau_{-} \times \Delta\lambda_{2}/\lambda_{2}$
ρ	$\Delta\rho = \rho \times \sqrt{\frac{\Delta N_1}{N_1}^2 + \frac{\Delta N_2}{N_2}^2}$

Table 6: Formulae used to propagate the statistical uncertainty upon the lifetimes and charge ratios obtained by *system.obtain_metrics*.

C Variation of the number of detected muons

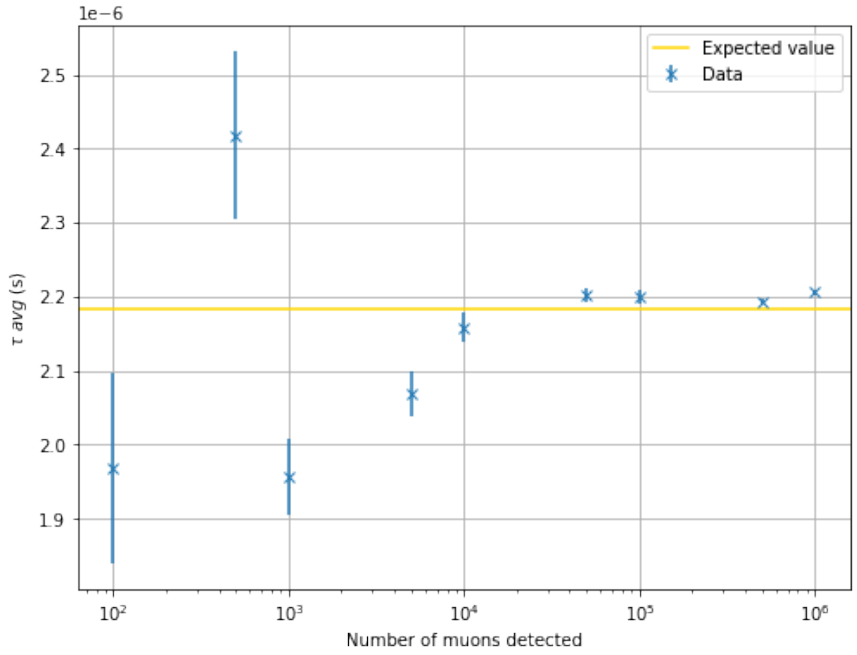

Figure 10: Variation of the lifetime parameter of the single exponential fit with number of muons detected.

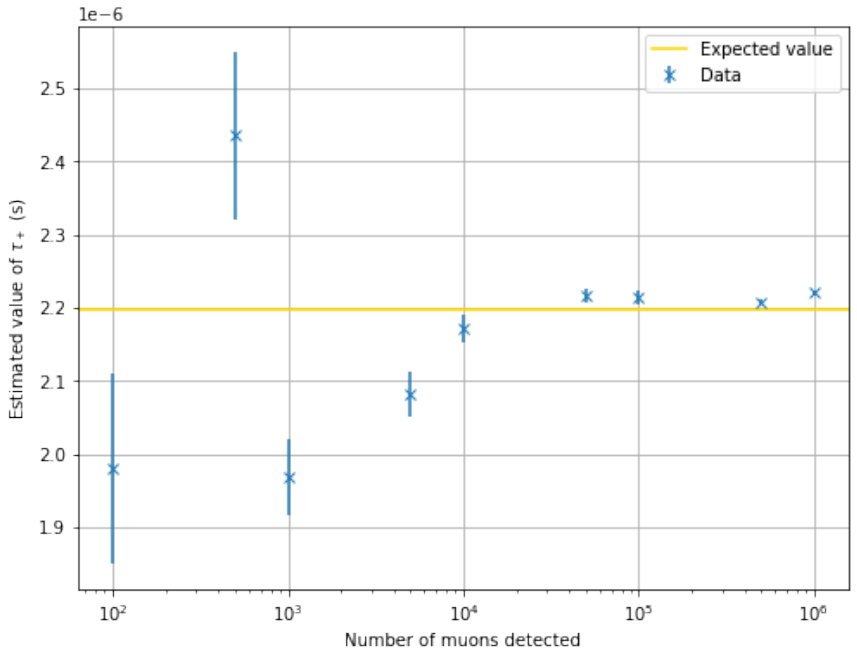

Figure 11: Variation of the positive muon lifetime estimated from the single exponential fit with number of muons detected.

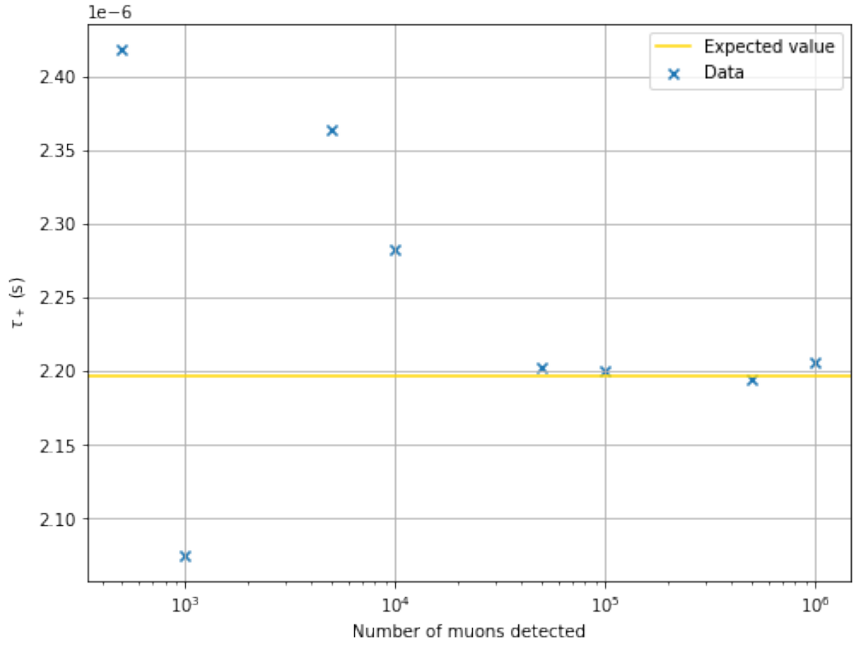

Figure 12: Variation of the positive muon lifetime with number of muons detected. Uncertainty upon these values is too large to plot on these axes, and is presented in Figure 14

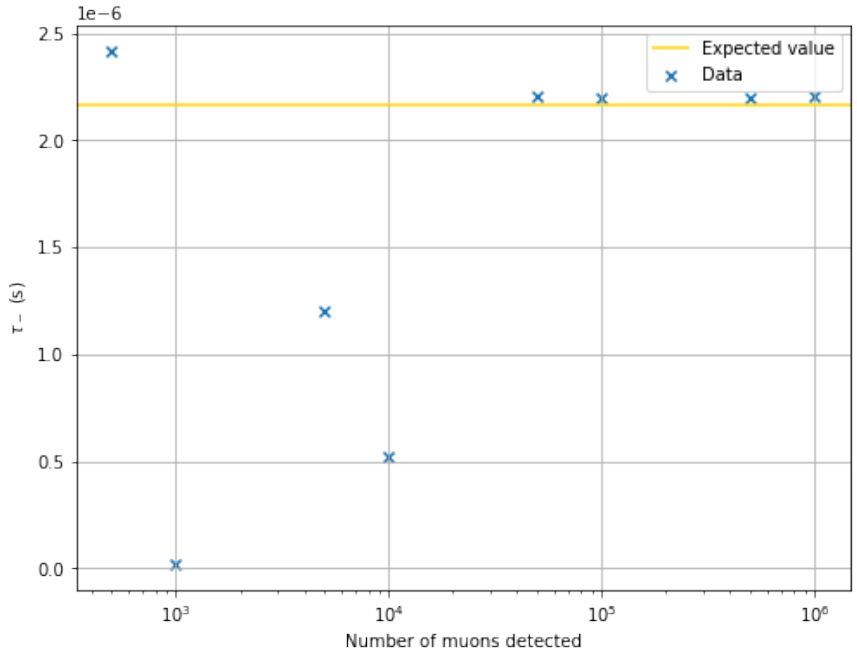

Figure 13: Variation of the negative muon lifetime with number of muons detected. Uncertainty upon these values is too large to plot on these axes, and is presented in Figure 14

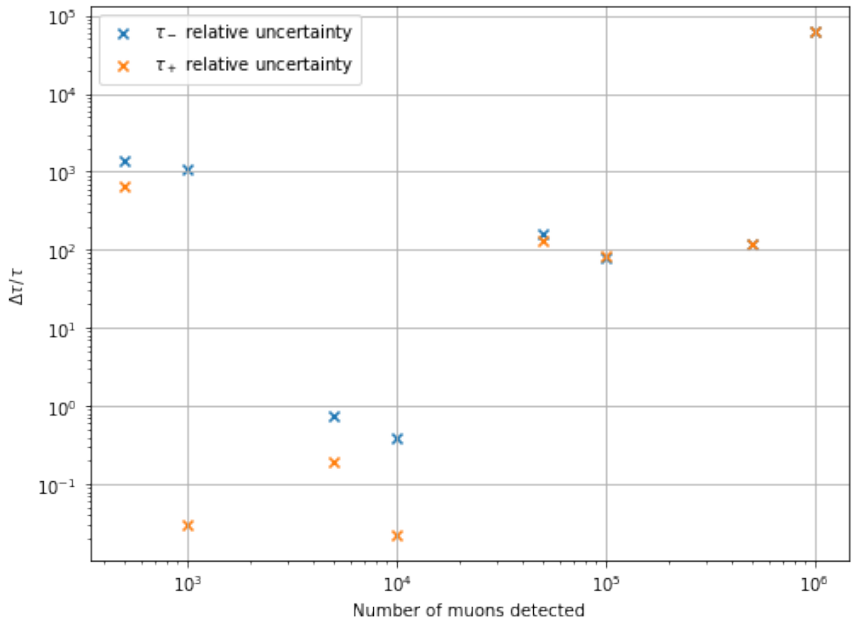

Figure 14: Variation of the relative uncertainty upon the positive and negative muon lifetimes produced from the double exponential fit with number of muons detected.

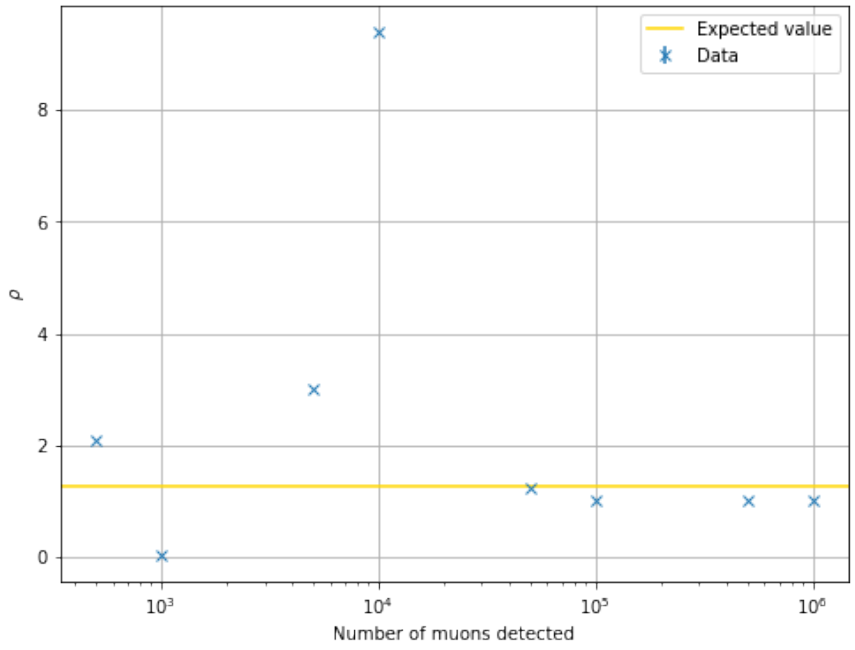

Figure 15: Variation of the charge ratio with number of muons detected. Uncertainties upon each value have been plotted, however they are too small to discern.